Repetitive Control and Online Optimization of Catofin Propane Process

Wangyun Won*, Kwang Soon Lee*†, Seokho Lee, and Chansul Jung****

**Department of Chemical and Biomoleulcar Engineering, Sogang University,Seoul, Korea (Tel: +82-2-705-8477; e-mail: kslee@sogang.ac.kr)*
***Samgsung Engineering Co., Ltd., Seoul, Korea (e-mail: sh.yi@samsung.com)*

Abstract: The Catofin propane process is an emerging industrial process for propylene production through dehydrogenation of propane. It is composed of multiple adiabatic fixed-bed reactors which undergo cyclic operations where propane dehydrogenation and catalyst regeneration alternate over roughly ten minute period for each. One of the major concerns in the operation of the Catofin process is maintaining the reactor at an optimum condition while overcoming gradual catalyst deactivation. Addressing this issue, an online optimization of the Catofin process combined with a repetitive control has been investigated. The optimizer computes optimum initial bed temperatures for dehydrogenation and optimum air flow rate for regeneration, and the repetitive controller performs cycle-wise feedback action during regeneration to attain the target bed temperatures at the terminal time of the regeneration period. Numerical studies have shown that the proposed online optimizing control system performs satisfactorily coping with the catalyst deactivation and other disturbances.

Keywords: Catofin process, online optimization, repetitive control, adiabatic fixed-bed reactor

1. INTRODUCTION

Advanced control and online optimization are now accepted as an essential process intensification technology that can create an additional profit in process industries wherever they are applicable. During the past two decades or more, there have been numerous industrial projects for advanced process control alone or integrated with online optimization as reviewed in Qin and Badgwell (2003). Such projects have typically proceeded for continuous processes with linear MPC only or cascaded by online steady state optimization. While the continuous process with steady state operation represents the majority of the chemical processes, non-continuous processes such as batch, semi-batch, and repetitive processes also take an important part. Such processes are run under unceasing dynamics, which renders conventional advanced control and online optimization techniques to show limitations in the performance. In this research, a repetitive process called the Catofin propane process (ABB, 2008) has been addressed and an advanced control technique combined with online optimization that exploits the unique nature of the Catofin process has been investigated.

In this study, an on-line optimizing control system for the Catofin propane process has been proposed and investigated numerically. The optimizing control system is composed of two tiers, a repetitive controller cascaded by an online optimizer. Repetitive control is put into an action during the regeneration (RG) steering the bed temperatures at two axial positions to reach the target values at the terminal time of the RG period. The open-loop operation with only a state estimation is conducted during the dehydrogenation (DH). The optimizer calculates the optimum target values for the bed temperatures and the RG air flow rate under a cyclic steady state. Both repetitive control and online optimization were constructed on the basis of a first principle reactor model reduced to a set of ordinary differential equations (ODE's) using the cubic spline collocation method (CSCM) (Yun and Lee, 2007). For the repetitive control, the model is linearized before the start of each RG cycle around the operating trajectories in the previous cycle. The performance of the proposed optimizing control scheme has been investigated numerically.

2. PROCESS DESCRIPTION

Fig. 1 shows a simplified process flow diagram of the Catofin propane process. It consists of multiple parallel adiabatic fixed-bed reactors that contain Cr_2O_3/Al_2O_3 catalyst, where the DH of propane and RG of catalyst are carried out alternatively over roughly ten minute period each with short periods of purging and evacuation operations in-between.

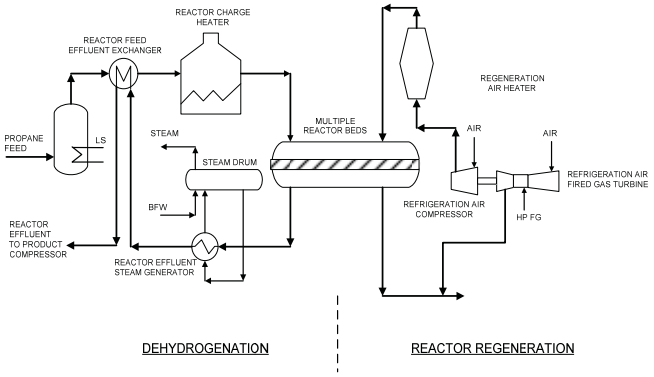

Fig. 1. Process flow diagram of the Catofin propane process.

The DH reaction is endothermic and produces a significant amount of coke. The bed temperatures are decreased and the catalyst loses activity by coke deposit and chromium reduction during this period. The RG reaction is coke burning by hot air and both the bed temperatures and catalyst activity are recovered under the oxidizing condition. The catalyst is known to have two years of life time and gradually loses the activity as the number of active sites is diminished by surface migration and agglomeration of Cr_2O_3 (Nijhuis, Tinnemans, Visser, and Weckhuysen, 2004).

The following apparent reaction kinetics proposed by Kim, Lee, and Song (1980) for the propane DH and Mickley, Nestor, and Gould (1965) and Pena, Monzon, and Santamaria (1993) for the coke combustion were assumed:

$$\begin{cases} C_3H_8 \underset{r_2}{\overset{r_1}{\rightleftharpoons}} C_3H_6 + H_2 \qquad C_3H_6 \xrightarrow{r_3} 3C + 3H_2 \\ C_3H_8 + C_3H_6 \xrightarrow{r_4} 2CH_4 + C_2H_6 + 2C \end{cases} \tag{1}$$

$$C + O_2 \xrightarrow{r_5} CO_2 \tag{2}$$

The rate constants are given in Table 1, which were slightly adjusted from the original values (Kim, Lee, and Song, 1980; Mickley, Nestor, and Gould, 1965; Pena, Monzon, and Santamaria, 1993) to more closely fit the conversion and yield of the real process (ABB, 2008).

Table 1. Parameters and normal operating conditions for the Catofin reactor model

Constants	Bed length = 1.5 (m), Bed diameter = 5.7 (m) C_c = 0.80 (kJ/kg•K), ρ_c=8x10^2 (kg/m^3), C_g = 3.71 for DH, 5.66 (kJ/kg•K) for RG D =1.7 for DH, 0.76 (m^2/min) for RG k_B=1.982 (kJ/min•m•K), R= 8.3462 (kJ/kmol K), DH and RG periods = 9min each
Normal operating condition for DH	Inlet temp=650℃, Propane flow=56.8(kmol/min), P=0.5 (atm)
Reaction rates (kmol/kg-cat.min) for DH	r_1= $k_1[C_3H_8]RT$, k_1=3.126*10^{7}e$^{(-47100/RT)}$ r_2=$k_2[C_3H_8][H_2]R2T2$, k_2=9.70*10^{-3}e$^{(-12800/RT)}$ r_3=$k_3[C_3H_6]R^2T^2$, k_3=8.407*10^{9}e$^{(-62900/RT)}$ r_4= k_4 $[C_3H_8][C_3H_6]R^2T^2$,k_4=9.498*10^{5}e$^{(-47800/RT)}$
Normal operating condition for RG	Inlet temp=690℃, Air flow=103.4 (kmol/min), P=2.0 (atm)
Reaction rate for RG	r_5=$k_5[C][O_2]RT$, k_5=4.129*10^{3}e$^{(-25575/RT)}$

It is assumed that the bed temperatures are measured at z = 0.2, 0.4, 0.6, 0.8, and 1.0, respectively, and the product gas compositions are available as the time average values over the DH and RG periods each with one cycle of measurement delay. It is also assumed that the RG is conducted under feedback control while the DH is carried out in an open loop state under a constant propane flow rate. The control objective during the RG is to steer the bed temperatures at z=0.2 and 0.4 to the target values provided by the optimizer using the RG air temperature as a manipulating variable (MV). The RG air flow rate was chosen as a decision variable for the optimizer together with the bed temperature target values.

3. REACTOR MODELLING

3.1 Mass and Energy Balances

In an adiabatic fixed-bed reactor, radial distribution of the concentrations and temperatures can be neglected. Under this assumption, the component mass and energy balance equations are written as

$$\begin{aligned} &\frac{\partial C_i}{\partial t} = \left(\frac{D}{L^2}\right)\frac{\partial^2 C_i}{\partial z^2} - \left(\frac{v_g}{L}\right)\frac{\partial C_i}{\partial z} + \left(\frac{1-\varepsilon}{\varepsilon}\right)\rho_c \bar{r}_i \\ &\frac{\partial C_c}{\partial t} = \rho_c \bar{r}_c \\ &\text{I.C. :} \quad C_i = C_i^I(z) \ \text{ at } \ t = 0 \\ &\text{B.C. :} \quad C_i = C_i^0(t) \ \text{ at } \ z = 0, \ \frac{dC_i}{dz} = 0 \ \text{ at } \ z = L_f = 5 \end{aligned} \tag{3}$$

$$\begin{aligned} &\frac{\partial T}{\partial t} = \left(\frac{k_B}{\rho_c c_{pc} L^2}\right)\frac{\partial^2 T}{\partial z^2} - \left(\frac{\varepsilon}{1-\varepsilon}\right)\left(\frac{\rho_g c_{pg} v_g}{\rho_c c_{pc} L}\right)\frac{\partial T}{\partial z} - \left(\frac{1}{c_{pc}}\right)\sum_j \Delta H_j r_j \\ &\text{I.C. :} \quad T = T_o(z) \ \text{ at } \ t = 0 \\ &\text{B.C. :} \quad T = T_o(\text{t}) \ \text{ at } \ z = 0, \ \frac{dT}{dz} = 0 \ \text{ at } \ z = L_f = 5 \end{aligned} \tag{4}$$

where $\bar{r}_i$ and C_i represent the rate of generation (kmol/kg-cat·min) and concentration (kmol/m^3) of component i, which refers to C_3H_8, C_3H_6, H_2, CH_4, C_2H_6 for DH operation, and CO_2, O_2 for RG operation, respectively; $\bar{r}_c$ and C_c represent the rate of generation (kmol/kg-cat·min) and concentration (kmol/m3) of coke, respectively; r_j referes to the rate of the j^{th} reaction; z denotes the normalized axial distance. Note that $\bar{r}_c$ for DH is different from $\bar{r}_c$ for RG. Other parameters and variables in the above model equations are given in Table 1.

In the above, the second boundary condition is specified at $z = 5$ instead of $z = 1$ whereas the spatial domain is $z \in (0,1]$. The reason for this is to more reasonably represent the true phenomenon, $dT/dz \to 0$ as $z \to \infty$, using a condition at a distant axial position, which was named as the far-side boundary condition (Yun and Lee, 2007).

3.2 ODE Models by Cubic Spline Collocation Method

ODE models for the virtual process and nominal model were derived separately using the CSCM (Yun and Lee, 2007) using ten and five equally spaced collocation points over

(0,1] plus an additional point at $z = 5$, respectively. The resulting ODE models can be concisely written as

$$\frac{d\bar{x}_k^i}{dt} = \bar{f}^i(\bar{x}_k^i, u_k^i), \quad i = DH, RG \tag{5}$$

In the above, the subscript k denotes the cycle number; $\bar{x}^{DH}$ represents the state for the DH model, that consists of bed temperatures, concentrations of C_3H_8, C_3H_6, H_2, CH_4, C_2H_6, and C at the internal collocation points; $\bar{x}^{RG}$ is similar to $\bar{x}^{DH}$ except that the concerned chemical components are C and O_2; u denotes the MV and represents the air temperature T^{air} for *i*=RG and is void for *i*=DH, respectively.

3.3 Process Behavior under a Cyclic Steady State

Fig. 2 shows the bed temperature trajectories of the virtual process under a cyclic steady state at the nominal operating condition. The bed temperatures are initially increased as the higher bed temperatures in the fore part of the respective collocation points recede by the gas flow. After a while, however, bed temperatures are decreased by the endothermic reactions as the propane DH proceeds and restored again by the coke combustion during the RG. The amount for the coke deposit changes during this operation are as shown in Fig. 3. The coke generation is larger at the higher temperature positions and vice versa.

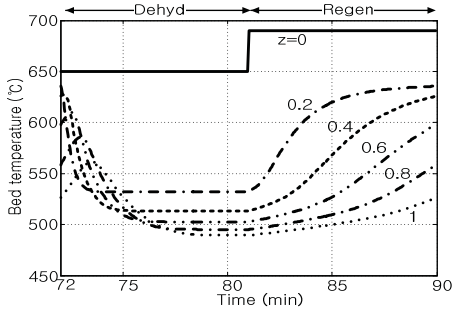

Fig. 2. Bed temperature trajectories at six axial positions under a cyclic steady state.

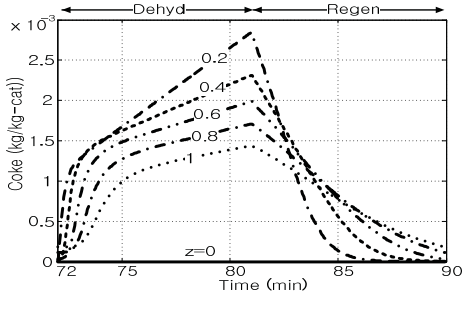

Fig. 3. Trajectories of coke deposit at six axial positions under a cyclic steady state.

The associated propane and propylene concentration trajectories during propane DH are shown in Fig. 4. Over an initial period while the bed temperatures are high, almost complete propane conversion and high propylene yield are obtained at the reactor outlet. As the bed temperatures begin to fall, both the propane conversion and propylene yield decrease. If we scrutinize Fig. 4, it can be seen that the front half of the bed where temperatures are higher than the rear half contribute more than 78.2% of the propylene production. The propane conversion and propylene selectivity averaged over a DH period are 51.5% and 86.2%, respectively.

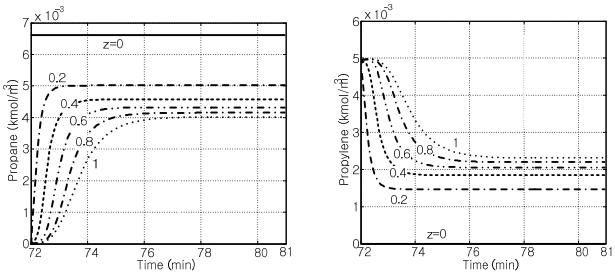

(a) (b)

Fig. 4. Trajectories of propane and propylene concentrations under a cyclic steady state.

4. OPTIMIZING CONTROL SYSTEM

4.1 Structure

The optimizing control system consists of three major parts: the online cyclic steady state optimizer, the repetitive controller, and the model estimator. Fig. 5 shows the overall structure of the proposed system.

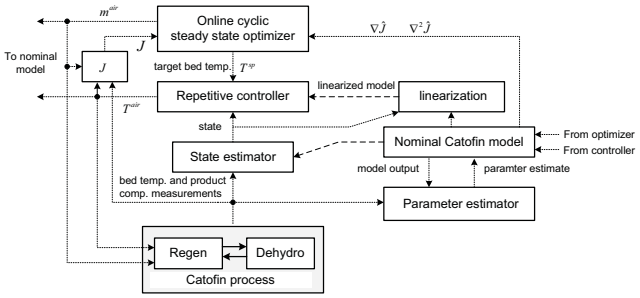

Fig. 5. Structure of the optimizing control system.

Fig. 6 illustrates the information flow through the state estimators along the operational sequence in more detail. The state estimation continues for the DH as well as RG periods based on the measurements of the bed temperatures and average product gas compositions in the previous cycle. Estimates of the coke deposit and bed temperature at the collocation points are transferred from the DH to RG and also from the RG to DH.

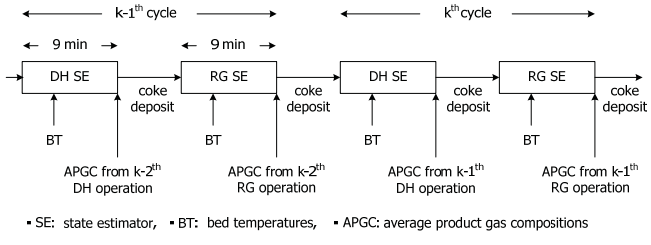

Fig. 6. Information flow along the sequence of operations.

4.2 Repetitive Control

4.2.1 Discrete-time Nominal Model

We first describe how the discrete-time nominal model for the state estimator and controller design is derived. The forward difference approximation applied to (5) results in

$$\bar{x}_k^i(t+1) = \bar{g}^i(\bar{x}_k^i(t), u_k^i(t)), \;\; i = \mathrm{DH}, \mathrm{RG} \tag{6}$$

The output equation can be written as

$$\begin{aligned} &\bar{y}_k^i(t) = V^i \bar{x}_k^i(t), \\ &\bar{p}_k^i = \frac{1}{N}\sum_{n=0}^{N-1} H^i \bar{x}_{k-1}^i(n), \;\; i = \mathrm{DH},\ \mathrm{RG} \end{aligned} \tag{7}$$

where $\bar{y}$ and $\bar{p}$ represent the bed temperatures at z=0.2, 0.4,…,1.0 and the average product gas composition measured at the end of the DH and RG periods with one cycle of measurement delay, respectively; N denotes the total number of sampling instance during the period of DH (or RG). V is a matrix that extracts the bed temperatures from the state and H is defined in a similar way for the compositions at the bed outlet. Hereafter, let us drop the superscript i for notational simplicity wherever there is no confusion.

The composition equation in (7) can be rewritten in the form of a state space equation. For this, let us define

$$\bar{p}_k(t+1) \triangleq \frac{1}{N}\sum_{n=0}^{t} H\, \bar{x}_{k-1}(n)$$

$$w_{1,k}(t) \triangleq \bar{x}_{k-1}(t), \;\; w_{2,k}(t) \triangleq \bar{x}_{k-1}(t+1), \cdots, w_{N,k}(t) \triangleq \bar{x}_k(t-1) \tag{8}$$

$$\bar{w}_k(t) \triangleq \begin{bmatrix} w_{1,k}(t) \\ w_{2,k}(t) \\ \vdots \\ w_{N-1,k}(t) \\ w_{N,k}(t) \end{bmatrix}, \; M \triangleq \begin{bmatrix} 0 & I & 0 & \cdots & 0 \\ 0 & 0 & I & \cdots & 0 \\ \vdots & \vdots & \ddots & \vdots & \vdots \\ 0 & 0 & 0 & \cdots & I \\ 0 & 0 & 0 & \cdots & 0 \end{bmatrix}, \; J \triangleq \begin{bmatrix} 0 \\ 0 \\ \vdots \\ 0 \\ I \end{bmatrix}, \; \bar{J} \triangleq \begin{bmatrix} I & 0 & \cdots & 0 & 0 \end{bmatrix}$$

Then the associated state transition equations are recast to

$$\begin{aligned} \bar{x}_k(t+1) &= \bar{g}(\bar{x}_k(t), u_k(t)) \\ \bar{w}_k(t+1) &= J\,\bar{x}_k(t) + M\bar{w}_k(t) \\ \bar{p}_k(t+1) &= \bar{p}_k(t) + \frac{1}{N} H\bar{J}\,\bar{w}_k(t) \end{aligned} \tag{9}$$

The resulting model equation can be rewritten in the following simplified form:

$$\begin{aligned} x_k(t+1) &= g(x_k(t), u_k(t)) \\ y_k(t) &= c(t) x_k(t) \end{aligned} \tag{10}$$

where

$$\begin{aligned} &x_k(t) \triangleq \begin{bmatrix} \bar{x}_k(t) \\ \bar{w}_k(t) \\ \bar{p}_k(t) \end{bmatrix}, \\ &y_k(t) = \bar{y}_k(t) \;\text{ and }\; c(t) = \begin{bmatrix} V & 0 & 0 \end{bmatrix} \quad \text{for } t = 1, \cdots, N-1 \\ &y_k(N) = \begin{bmatrix} \bar{y}_k(N) \\ \bar{p}_k(N) \end{bmatrix} \text{ and } c(N) = \begin{bmatrix} V & 0 & 0 \\ 0 & 0 & I \end{bmatrix} \end{aligned} \tag{11}$$

Note that (10) and (11) holds for DH and RG separately.

4.2.2 Control Algorithm for RG Operation

The repetitive control conducts cycle-wise integral control action. To facilitate the construction of the control law, it is convenient to transform (10) to a state space model with $\Delta u_k(t) \triangleq u_k(t) - u_{k-1}(t)$ and $y_k(t)$ as the input and output variables, respectively. Linearization of (10) around the trajectories of the process variables in the k-1$^{\text{th}}$ cycle yields

$$\begin{aligned} \Delta x_k(t+1) &= A_{k-1}(t)\Delta x_k(t) + B_{k-1}(t)\Delta u_k(t) \\ y_k(t) &= y_{k-1}(t) + C_{k-1}(t)\Delta x_k(t) \end{aligned} \tag{12}$$

where $\Delta x_k(t) \triangleq x_k(t) - x_{k-1}(t)$; $A_{k-1}(t)$ represents a shorthand notation of $A_{k-1}(u_{k-1}(t), x_{k-1}(t\,|\,t))$, and similarly for $B_{k-1}(t)$ and $C_{k-1}(t)$. $\Delta u_k(t)$ is allowed to change P times at $t_1(=0)$, t_2, $\cdots, t_P$ during the RG period and determined at each time moment to satisfy the following quadratic prediction objective:

$$\begin{aligned} &\min_{\Delta u_k(\bullet)} \left[\left\| T_k^{sp} - \hat{y}_k(N\,|\,t_m) \right\|_Q^2 + \sum_{n=m}^{P} \left\| \Delta u_k(t_n) \right\|_{R(m)}^2 \right], \;\; m = 1, \cdots, P \\ &\text{subject to input constraints} \end{aligned} \tag{13}$$

At other occasions than t_m, $m = 1, \cdots, P$ $\Delta u(t) = 0$. In the above, $\hat{y}_k(N\,|\,t_m)$ represents a prediction of $\hat{y}_k(N)$, the bed temperatures at z=0.2 and 0.4, on the basis of the information up to t_m at the k^{th} cycle; T_k^{sp} denotes the target value of $\hat{y}_k(N)$. $\hat{y}_k(N\,|\,t_m)$ is given by the following form:

$$\hat{y}_k(N\,|\,t_m) = \hat{y}_{k-1}(N) + F_{k-1}(t_m)\Delta x_k^{RG}(t_m\,|\,t_m) + \sum_{n=m}^{P} G_{k-1}(t_n)\Delta u_k(t_n) \tag{14}$$

It is straightforward to derive (14) from (12). Note that the state estimate $x_{k-1}(t\,|\,t)$ and $\Delta x_k^{RG}(t_m\,|\,t_m)$ are needed to construct (12) (for linearization) and to solve (13) for $\Delta u_k(\bullet)$ (using (14)), respectively.

4.2.3 State Estimator

The state estimator is constructed separately for DH and RG in the form of the extended Kalman filter (EKF) for (10) and is given as

$$\begin{aligned} x_k(t+1\,|\,t) &= g\left(x_k(t\,|\,t), u_k(t)\right) \\ x_k(t\,|\,t) &= x_k(t\,|\,t-1) - K_k(t)\left(y_k(t) - c_k(t) x_k(t\,|\,t-1)\right) \end{aligned} \tag{15}$$

The observer gain $K_k(t)$ was obtained according to the EKF law using the process and measurement noise covariance matrices as the tuning factors. Using $x_k^{RG}(t_m\,|\,t_m)$ and $x_{k-1}^{RG}(t_m\,|\,t_m)$, $\Delta x_k^{RG}(t_m\,|\,t_m) = x_k^{RG}(t_m\,|\,t_m) - x_{k-1}^{RG}(t_m\,|\,t_m)$ for (14) was estimated. The state estimator acts as a fixed-lag smoother at t=N because the average product gas compositions are measured with one cycle of delay.

4.2.4 Implementation procedure

Over a DH-RG cycle, the following steps take turns in the repetitive control level:

[Step 1] DH period

$x_k^{DH}(t\,|\,t)$ is estimated for $t = 1, \cdots, N$ using (15).

[Step 2] Transition from DH to RG

Initialize $x_k^{RG}(1\,|\,0)$ by carrying over the coke deposit and bed temperature estimates in $x_k^{DH}(N\,|\,N)$ to $x_k^{RG}(1\,|\,0)$. Obtain the linearized model in (12) by linearizing (10) around $x_{k-1}^{RG}(t\,|\,t)$ and $u_{k-1}(t-1)$, $t = 1, \cdots, N$.

[Step 3] RG period

Perform the state estimation using (15). Compute $\Delta x_k^{RG}(t\,|\,t) = x_k^{RG}(t\,|\,t) - x_{k-1}^{RG}(t\,|\,t)$. Determine $\Delta u_k(t_m)$, $m = 1, \cdots, M$ according to (13) and (14). Implement $T_k^{air}(t) = u_k(t) = u_{k-1}(t) + \Delta u_k(t)$ to the process.

[Step 4] Transition from RG to DH

Initialize $x_k^{DH}(1\,|\,0)$ by transferring the coke deposit and bed temperature estimates in $x_k^{RG}(N\,|\,N)$ to $x_k^{DH}(1\,|\,0)$.

4.3 Online Cyclic Steady State Optimizer

The online optimizer determines T^{sp} and m^{air}, the target bed temperatures and the combustion air flow rate, respectively, that minimize the cost function under a cyclic steady state whenever the optimizer is invoked.

$$\begin{aligned}
&\min_{T^{sp}, m^{air}} J = -\alpha_1 m^p Y_{css}^p + \alpha_2 \sum_{t=1}^{N} c_{pa} m^{air} \left(T_{css}^{air}(t) - T_{ref} \right) \\
&\qquad + \alpha_3 \left(\max(0, T_{z=0.2}^{sp} - 500) \right)^2 + \|s\|_Q^2, \quad a_i > 0, \quad Q > 0 \\
&\text{subject to} \quad (10) \\
&\qquad \begin{bmatrix} 615 \\ 600 \end{bmatrix} \le T^{sp} \le \begin{bmatrix} 720 \\ 690 \end{bmatrix} (^\circ\text{C}) \\
&\qquad 10 \le \left| T_{z=0.2}^{sp} - T_{z=0.4}^{sp} \right| \le 30 (^\circ\text{C}) \\
&\qquad m_{\min}^{air} \le m^{air} \le m_{\max}^{air} \\
&\qquad s = x^{DH}(0) - x^{RG}(N)
\end{aligned} \tag{16}$$

where T_{ref}, m^p, and Y^p represent the reference temperature, propane mass flow rate, and average propylene yield over a DH period, respectively and the subscript *css* means the cyclic steady state. The summation is taken over the RG period.

The last term in J is to enforce the cyclic steady state condition, which is slackened by introducing a slack variable *s* defined the last equation in (16).

4.4 Model Parameter Estimator

In this study, the catalyst deactivation was assumed to be the most important process change and the parameter estimator was designed to update the pre-exponent rate constants by minimizing the following quadratic objective on the prediction error:

$$\min_{\theta^i} V^i = \frac{1}{k_2 - k_1} \sum_{k=k_1}^{k_2-1} \sum_{t=1}^{N} \left\| y_k^{m,i}(t) - y_k^i(t;\theta^i) \right\|_{\bar{Q}}^2, \; i = \text{DH, RG} \tag{17}$$

$$\text{subject to} \quad \theta_{\min}^i \le \theta^i \le \theta_{\max}^i$$

where $y_k^{m,i}(t)$ and $y_k^i(t;\theta^i)$ represent the measurement and model prediction of $y_k^i(t)$ based on θ^i, respectively.

We devised a three parameter function as in (18), which is to be multiplied to each of the pre-exponent rate constants.

$$\xi(z) = \begin{cases} a + b\left(1 + \sin\left((-\pi / 2d)(z + d)\right)\right), & z \in [0,1] \\ a + 2b \quad \text{if } 2d \le z \end{cases} \tag{18}$$

Since there are four rate constants for the DH, $\theta^{DH} \triangleq \left[a_1 \cdots a_4 \; b_1 \cdots b_4 \; d_1 \cdots d_4\right]$. Likewise, $\theta^{RG} \triangleq \left[a_5 \; b_5 \; d_5\right]$.

It is true that (18) is only a rough description of the catalysts activity distribution in the real process. Nonetheless, both the repetitive controller and the optimizer can achieve highly precise tracking as well as the true minimum, respectively, overcoming model uncertainties since the controller performs the cycle-wise integral action and the optimizer searches for the minimum on the basis of the process measurements.

5. SIMULATION CONDITIONS

The sampling period was chosen to be 3 sec resulting in total sampling instants of 360 with $t^{RG} = t^{DH} = 180$ over an entire cycle. The number control moments *P* was chosen as 3 and t_1, t_2, and t_3 were selected as 1, 60, and 120, respectively. The following constraints were imposed on the MV movements for repetitive control:

$$600 \le u(t) = T_{air}(t) \le 750 (^\circ\text{C}) \tag{19}$$

In the virtual process, the case of catalyst deactivation is represented by multiplying all k_i's by $1 - 0.5e^{-2.4z}$.

6. RESULTS AND DISCUSSION

The performance of the optimizing control system has been investigated for two cases. In the first case, the reactor was assumed to be initially at an arbitrary open-loop cyclic steady state and the optimizer steers the reactor to an optimum condition. In this case, the model parameter estimator was not invoked. In the second case, the optimum operation condition was assumed to be changed by catalyst deactivation, and the optimizer seeks for a new optimum condition from the previous operating condition determined in the first case. In the second case, the model parameter estimator plays an important role for both the repetitive controller and the online optimizer.

The simulation results for the first case are summarized in Fig. 7. It shows the response of the bed temperatures to their respective target values sent by the optimizer and the decrease of the objective function as the online optimization proceeds. The online optimizer calculates the new optimal target values once a cyclic steady state is reached on the basis of the nominal model and process measurements whereas the repetitive controller maneuvers the air temperature to attain the target values.

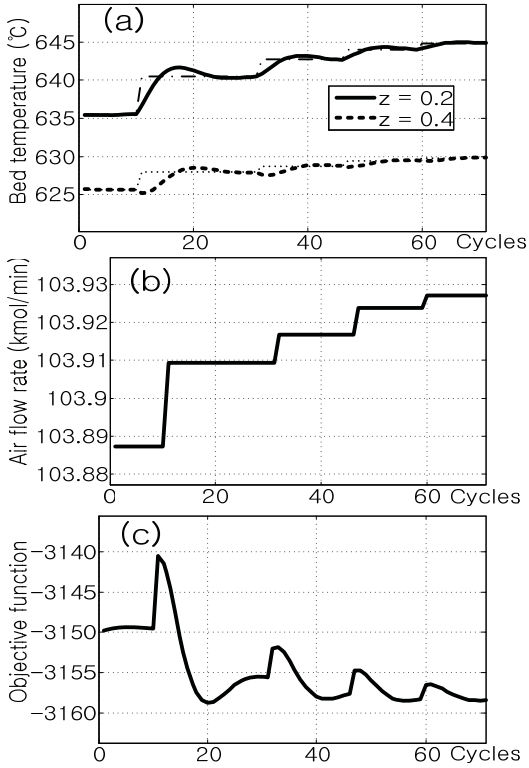

Fig. 7. Results of online optimization starting from an arbitrary open-loop state; (a) bed temperatures and their target values, (b) combustion air flow rate, (c) objective function.

The simulation results for the second case are given in Fig. 8. It can be seen that the overall responses are similar to Fig. 7. Unlike in the previous case, however, θ^{DH} and θ^{RG} were recurrently updated during the optimization. One thing to note is that the bed temperatures are raised even higher from the values determined in the first case to compensate for the catalyst deactivation.

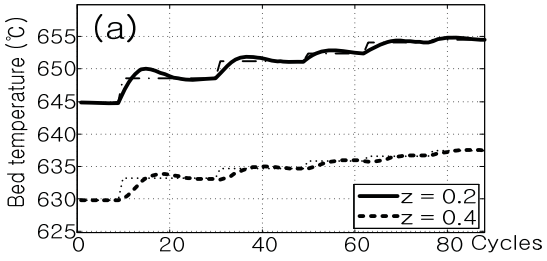

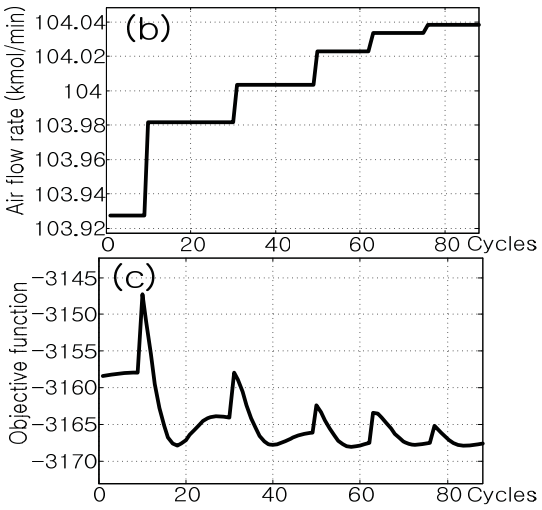

Fig. 8. Results of online optimization after the catalyst deactivation occurs; (a) bed temperatures and their target values, (b) combustion air flow rate, (c) objective function.

REFERENCES

ABB (2008). http://www02.abb.com/GLOBAL/NOOFS/noofs187.nsf/viewunid/494CDF435B2EE22DC12569EE0036977A/$file/CATOFIN.pdf

Bhasin, M. M., McCaina, J. H., Vora, B. V., Imai, T., & Pujad, P. R. (2001). Dehydrogenation and oxydehydrogenation of paraffins to olefins. *Applied Catalysis A: General*, 221, 397–419.

Kim, Y. G., Lee, H. S., & Song, Y. S. (1980). A study on dehydrogenation of propane. *Korean Journal of Chemical Engineering*, 18, 11-19.

Mickley, H. S., Nestor, J. W., & Gould, L. A. (1965). A kinetic study of the regeneration of a dehydrogenation catalyst. *Canadian Journal of Chemical Engineering*, 61-68.

Nijhuis, T. A., Tinnemans, S. J., Visser, T., & Weckhuysen, B. M. (2004). Towards real-time spectroscopic process control for the dehydrogenation of propane over supported chromium oxide catalysts. *Chemical Engineering Science*. 59, 5487-5492.

Pena, J. A., Monzon, A., & Santamaria, J. (1993). Coking kinetics of fresh and thermally aged commercial Cr2O3/Al2O3 catalyst. *Applied Catalysis A*, 101, 185-198.

Qin, S. J. & Badgwell, T. A. (2003). A survey of industrial model predictive control technology. *Control Engineering Practice*, 11, 733-764.

Yun, W. & Lee, K. S. (2007). The Use of Cubic Spline and Far-side Boundary Condition for the Collocation Solution of a Transient Convection-Diffusion Problem. *Korean Journal of Chemical Engineering*, 24, 204-208.